Soft physics observables in heavy ion collisions

Francesco Prino

INFN, Sezione di Torino

Abstract. Soft (i.e. low momentum) hadrons constitute the bulk of the particles produced in relativistic heavy ion collisions and they are therefore essential to characterize the system created in these reactions. For the more central (i.e. small impact parameter) collisions and/or at the larger center-of-mass energies, where the higher temperatures and energy densities are attained, it is expected on the basis of lattice QCD calculations that the produced matter can reach the conditions for deconfining quarks and gluons on volumes much larger than the hadronic size. The system in its early stages is therefore expected to be composed of deconfined partons which hadronize when the critical temperature is reached during the expansion and cooling of the system. In this contribution, three experimental observables which can be studied with the statistics collected in the first few hours of data taking of an heavy-ion experiment will be discussed. The first observable is the pseudorapidity distribution of charged particles which is related to the energy density attained in the collision. The second is the multiplicity of identified hadrons which, in the framework of statistical hadronization models, allows to extract the temperature and the baryonic density of the system at the chemical freeze-out. Finally, the azimuthal distribution of produced particles is discussed: the presence of anisotropic patterns in the transverse plane indicates that enough rescatterings occurred in the early stages of the system evolution and that the produced particles underwent a collective motion (flow) until the moment of the thermal freeze-out.

Keywords: Heavy ion collisions, particle production, flow
PACS: 25.75.Ag, 25.75.Dw, 25.75.Ld

CHARGED PARTICLE PSEUDORAPIDITY DISTRIBUTIONS

The number of particles (multiplicity) produced in heavy-ion collisions quantifies to which extent the incoming beam energy is released to produce new particles and brings information about the entropy of the system and the gluon density in the first stages of the collision evolution. Furthermore, it is related to the impact parameter, i.e. to the centrality of the collision: more particles are produced in central (small impact parameter, many elementary nucleon-nucleon collisions) than in peripheral reactions.

Experiments usually characterize the event multiplicity from the pseudorapidity ($\eta = -\ln[\tan(\vartheta/2)]$) distributions of charged particles. The measurement of $dN_{\rm ch}/d\eta$ as a function of the energy and the centrality of the collision may also help to constrain different models of particle production. On this respect, it should be pointed out that particle production in hadronic collisions is dominated by soft (non-perturbative) processes and consequently an understanding of multiplicities based on first principles is missing.

The $dN_{\rm ch}/d\eta$ distributions at RHIC present typical trapezoidal shapes [1], with maximal density of particles in the midrapidity region (around $\eta = 0$ at colliders). SPS (fixed-target) experiments observed Gaussian shaped $dN_{\rm ch}/d\eta$ peaked at midrapidity ($\eta \approx y_{beam}/2$ in the laboratory system) [2]. The different shape between fixed-target and collider experiments is due to the fact that η is not Lorentz invariant.

Particle yield at mid-rapidity

The pseudorapidity density of charged particles at mid-rapidity ($dN/d\eta\ |_{\eta=0}$) is commonly used to characterize the event multiplicity because it allows a comparison between different experiments, being independent of the detailed phase-space acceptance. A convenient variable to study the scaling of particle production with centrality and energy is the yield per participant pair at mid-rapidity, $dN/d\eta\ |_{\eta=0}/(N_{\text{part}}/2)$, which for soft particles, scaling with N_{part} [3], is expected to be independent of centrality and self-normalized to p-p collisions. RHIC data show an increasing yield per participant pair with increasing centrality (about 25% increase from mid-peripheral to central collisions) at all energies, as it can be seen in fig. 1-a. The explanation of this increase as due to the contribution of hard processes (scaling with the number of collisions) is contradicted by the observation that the ratios of the measured yields at two different energies are independent of centrality. A factorization of the energy and centrality (geometry) dependence of the charged particle pseudorapidity densities is observed.

Particle yields at mid-rapidity measured at RHIC are well described by models based on parton saturation either in the initial state [4, 5] or in the produced gluons [6] This suggests that high density QCD effects play an important role in determining the global event features at RHIC energies. As an example, the curves from [4], with only one free parameter adjusted on RHIC data, are shown in fig. 1-a superimposed to the experimental points. However, as pointed out in [8], different models to calculate N_{part} (which is not a direct experimental observable and affects both axes of fig. 1-a) would lead to different slopes for the centrality dependence of the yield per participant pair. Differences in N_{part} calculation may explain also why the yield per participant pair is found to be almost flat as a function of centrality at $\sqrt{s}$=17.2 GeV by SPS experiments [2] and increasing with centrality at $\sqrt{s}$=19.6 GeV by PHOBOS at RHIC.

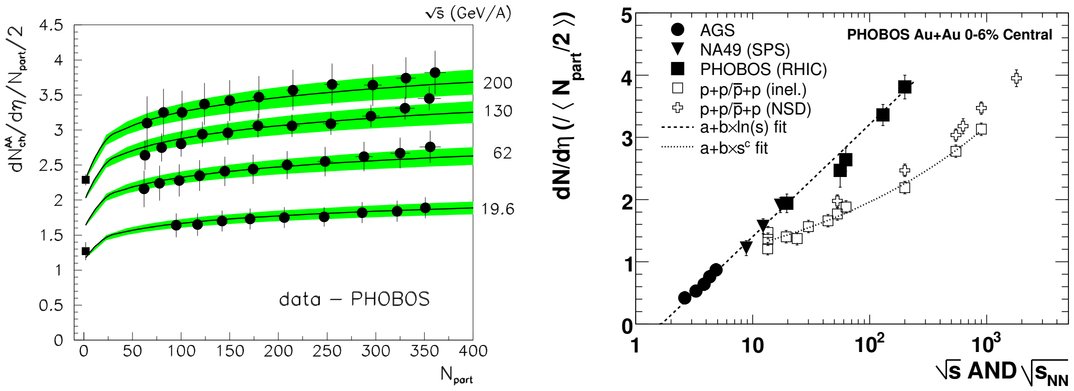

(a) (b)

FIGURE 1. (a) Pseudorapidity density of charged particles at midrapidity per participant pair as a function of centrality at RHIC together with saturation model [4] (taken from [9]) (b) Energy dependence of the pseudorapidity density of charged particles per participant pair (in the center-of-mass frame) for the most central ion-ion collisions from AGS to RHIC (taken from [7]). pp($\bar{\text{p}}$) data are superimposed.

The $dN/d\eta\ |_{\eta=0}$ per participant pair as a function of $\sqrt{s}$ for central heavy-ion collisions from AGS to RHIC energies is shown in fig 1-b together with proton-proton data. The multiplicities at midrapidity in central heavy-ion collisions follow a different trend with respect to pp($\bar{\mathrm{p}}$) reactions. The measured yield per participant pair increases logarithmically with $\sqrt{s}$ in the entire range covered by the AGS, SPS and RHIC experiments. The extrapolation of this trend to the 3% most central Pb-Pb collisions at the LHC ($\sqrt{s} = 5.5$ TeV) leads to $dN/d\eta\ |_{\eta=0}(LHC) = 1200 \pm 100$ [9]. Models based on saturation predict a stronger (power-law) dependence on $\sqrt{s}$ resulting in larger predictions for multiplicity at the LHC, namely 1650 from [4], 2200 from [5], 2570 from [6]. The first 10,000 events at the LHC will allow to discriminate among these models.

Starting from the measured values of $dN/d\eta\ |_{\eta=0}$ and using the Bjorken formula [10] (although a boost-invariant central plateau is not observed also at top RHIC energy [11]), it is possible to estimate the energy density attained in the collision. At top RHIC energy ($\sqrt{s} = 200$ GeV), one obtains $\varepsilon_{BJ} \approx$9 GeV/fm^3 at the estimated equilibration time ($\approx$0.6 fm/c), well above the critical value predicted by lattice QCD for the phase transition to a state of deconfined partons(for a detailed discussion, see [12]).

Particle production in the fragmentation regions

The forward and backward regions of the pseudorapidity distributions, i.e. the regions close to beam rapidities where $p_{\mathrm{L}} \gg p_{\mathrm{T}}$, allow to investigate effects connected with projectile and target fragmentation. In particular, the limiting fragmentation hypothesis [13] states that at high enough collision energy both the particle spectra and the mix of particle species reach a limiting value and become energy independent in a region around the projectile (and target) rapidity. This effect implies also a limiting value for the $dN_{\mathrm{ch}}/d\eta$ which is expected to be energy independent in a region around the beam rapidity.

For this analysis, it is convenient to consider the particle distributions in the rest frame of one of the two colliding nuclei by introducing the variable $\eta' = \eta - y_{beam}$. The results obtained by PHOBOS [1] show that the particle distributions in the fragmentation regions follow a common limiting curve independent of collision energy over a wide η' range. Furthermore, the extent of this “limiting fragmentation region” grows significantly with increasing energy and at $\sqrt{s}$=200 GeV it extends more than two units away from the beam rapidity. This result is in contrast to the boost-invariance scenario [10] which predicts a broad plateau at mid-rapidity growing in extent with increasing beam energy. The measured pseudorapidity distributions appear to be dominated by two “fragmentation” regions, whose extent increases with collision energy. The extrapolation of this universal extended longitudinal scaling to LHC energy is reported in fig. 2. The persistence of this scaling limits the maximum attainable multiplicity at $\sqrt{s} = 5.5$ TeV to about 1600-1700 particles per unit of rapidity and therefore it can not be reconciled with the predictions from saturation models [4, 5, 6] tuned on RHIC data, unless in the case of a strong deviation of the $dN_{\mathrm{ch}}/d\eta$ distributions from the characteristic trapezoidal shape observed at RHIC energies. So, as pointed out in [14], either the universal extended longitudinal scaling will be broken at the LHC, or the saturation models advocated to explain the multiplicities measured at RHIC will have to be revisited.

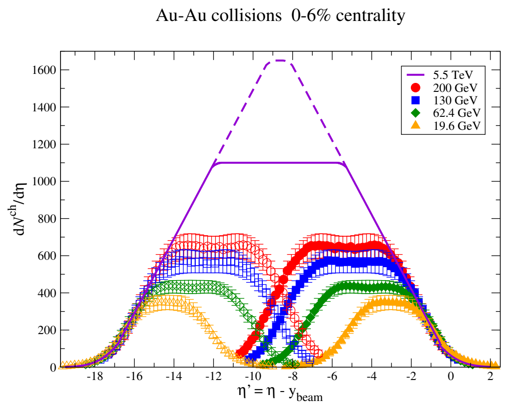

FIGURE 2. $dN_{\mathrm{ch}}/d\eta$ distributions for Au-Au collisions at RHIC plotted in the rest frame of one of the colliding nuclei and reflected about LHC midrapidity. Extrapolations to LHC based on self-similar trapezoidal shape (logarithmic extrapolation) of $dN_{\mathrm{ch}}/d\eta$ distributions (solid line) and saturation model [4] are shown (taken from [14]).

Total charged multiplicity

The total charged multiplicity (N_{ch}) per participant pair (obtained by PHOBOS by integrating the measured $dN_{\mathrm{ch}}/d\eta$ distributions) is shown as a function of centrality in fig. 3-a for three different RHIC energies. Contrarily to the $dN/d\eta\,|_{\eta=0}$, the total charged multiplicity results to be proportional to the number of participant nucleons. This scaling with N_{part} comes from a compensation between the narrowing of the $dN_{\mathrm{ch}}/d\eta$ distributions and the increasing of $dN/d\eta\,|_{\eta=0}/(N_{\mathrm{part}}/2)$ with increasing centrality. The charged multiplicity per participant pair in Au-Au collisions at RHIC agrees with the one measured in $\mathrm{e}^+\mathrm{e}^-$, and not in $\mathrm{pp}(\bar{\mathrm{p}})$, collisions at the same energy. This is also visible in fig. 3-b where N_{ch} per participant pair from central heavy-ion collisions at AGS, SPS and RHIC is plotted together with $\mathrm{pp}(\bar{\mathrm{p}})$ and $\mathrm{e}^+\mathrm{e}^-$ data.

The fact that $\mathrm{pp}(\bar{\mathrm{p}})$ multiplicities lie about 30% below the $\mathrm{e}^+\mathrm{e}^-$ data at the same energy is attributed to the "leading particle effect": the outgoing proton carries away a substantial amount of the beam energy, thus reducing the energy effectively available for particle production [15]. The multiplicities measured in $\mathrm{pp}(\bar{\mathrm{p}})$ and $\mathrm{e}^+\mathrm{e}^-$ reactions become consistent over a broad energy range if the effective energy ($\sqrt{s_{eff}} = \sqrt{s}/2$) is introduced for $\mathrm{pp}(\bar{\mathrm{p}})$ collisions to account for the leading particle effect.

Heavy ion multiplicities do not follow the $\mathrm{e}^+\mathrm{e}^-$ trend over the whole $\sqrt{s}$ range. Instead, they lie below the $\mathrm{pp}(\bar{\mathrm{p}})$ data at AGS energies, cross through the $\mathrm{pp}(\bar{\mathrm{p}})$ curve around $\sqrt{s} \sim 10$ GeV and then gradually join the $\mathrm{e}^+\mathrm{e}^-$ multiplicities above the SPS energies. At RHIC energies, the multiplicity per participant pair in heavy-ion collisions agrees with the one observed in $\mathrm{e}^+\mathrm{e}^-$ reactions at the same $\sqrt{s}$, suggesting a substantially reduced leading particle effect in central heavy-ion reactions at high energy due to the the multiple collisions suffered by each participating nucleon [16]. The "suppression" of A-A multiplicity with respect to $\mathrm{e}^+\mathrm{e}^-$ at lower energies is possibly explained by the larger number of baryons produced at such energies which tends to suppress the over-

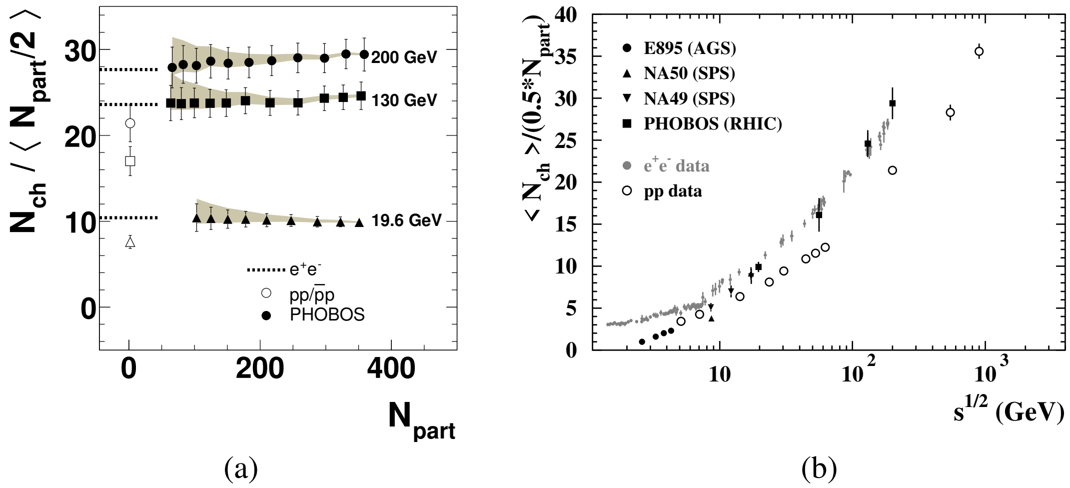

FIGURE 3. (a) Centrality dependence of the total charged multiplicity per participant pair as measured by PHOBOS experiment at $\sqrt{s}$=19.6, 130 and 200 GeV (taken from [16]). (b) Energy dependence of the total charged multiplicity per participant pair for the most central ion-ion collisions from AGS to RHIC. pp($\bar{\text{p}}$) and e^+e^- data are superimposed.

all multiplicity, due to the fact that the baryo-chemical potential reduces the entropy [1]. These considerations suggest that the total multiplicity per participant pair might be a universal function of the available energy, irrespectively of the colliding system.

HADRON ABUNDANCES

The measurement of the multiplicities of identified hadron species allows to get insight into the characteristics of the system at the instant of chemical freeze-out, when the inelastic collisions cease and particle abundances are frozen. The hadron multiplicities in heavy ion collisions are reproduced in the energy range from SIS/GSI ($\sqrt{s} \approx 2$ GeV) to RHIC ($\sqrt{s} \approx 200$ GeV) by statistical/thermal models (see e.g. [17]) under the assumption that the hadronization occurs following a purely statistical (entropy maximization) law. The hadronic system is described by a gas of non-interacting hadrons and resonances in chemical and thermal equilibrium, without specifying how and when during the evolution of the fireball this equilibrium is reached. For central heavy-ion collisions the grand-canonical formulation of statistical mechanics is used. The temperature T and baryo-chemical potential μ_B at chemical decoupling are extracted from a fit to the measured particle (relative) abundances. For smaller systems (e^+e^-, pp($\bar{\text{p}}$)) where exact conservation of quantum numbers is required, the canonical or micro-canonical formulations are used [18]. The success of the thermal models in explaining the measured hadron abundances over two orders of magnitude of $\sqrt{s}$ indicates that hadron production is dominated by phase space rather than by microscopic dynamics.

The obtained results for the fit parameters (to particle ratios and yields at midrapidity in AA collisions and to 4π multiplicities in e^+e^- and pp($\bar{\text{p}}$)) are shown in fig. 4 as

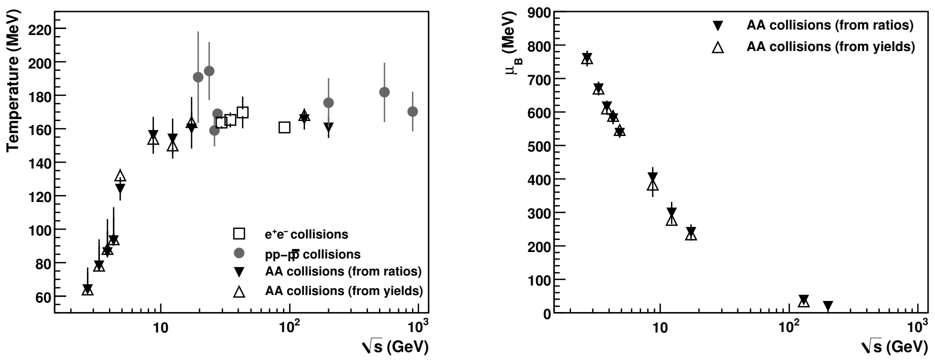

FIGURE 4. Temperature and baryo-chemical potential (extracted from thermal model based fits to hadron abundances) as a function of $\sqrt{s}$. Data taken from [17, 18]

a function of the center-of-mass energy. The baryo-chemical potential (which is not defined in the case of e^+e^- and $pp(\bar{p})$ collisions where the canonical ensemble is used) decreases by about one order of magnitude from SPS to RHIC collisions and is expected to be very small ($\ll$ 10 MeV) at the LHC, in agreement with the expectation of an almost net-baryon free region at midrapidity. The chemical freeze-out temperature in A-A collisions reaches a $\sqrt{s}$-independent limiting value of $\approx$160-170 MeV in the SPS energy range. It is interesting to note that compatible values of temperatures are obtained in e^+e^- and $pp(\bar{p})$ reactions. This observed "universal" (i.e. independent of energy and colliding system) limiting value of $\approx$ 170 MeV for the chemical freeze-out temperature suggests that hadronization occurs when the parameters of prehadronic matter drop below critical values and that above these values no hadronic phase-space exists [18]. This limiting temperature agrees within errors with the one predicted by lattice QCD for the phase transition to a deconfined state and with the Hagedorn limiting temperature for an equilibrated hadron gas [19].

ELLIPTIC FLOW

In heavy-ion collisions with non-zero impact parameter, the rotational symmetry around the beam axis is broken and the impact parameter defines a preferred direction in the transverse plane. As a consequence, the azimuthal distribution of the produced particles may result to be anisotropic with respect to the reaction plane (defined by the impact parameter itself and the beam axis). The particle azimuthal distributions relative to the reaction plane are usually written in the form of Fourier series as:

$$\frac{dN}{d\varphi} = \frac{1}{2\pi}\left(1 + \sum_{n=1}^{\infty} 2v_n \cos[n(\varphi - \Psi_{RP})]\right) \tag{1}$$

where Ψ_{RP} is the angle defined by the impact parameter vector in the transverse plane. The v_n coefficients are given by $v_n = \langle\cos[n(\varphi - \Psi_{RP})]\rangle$. The first two coefficients v_1 and v_2 are called directed and elliptic flow respectively.

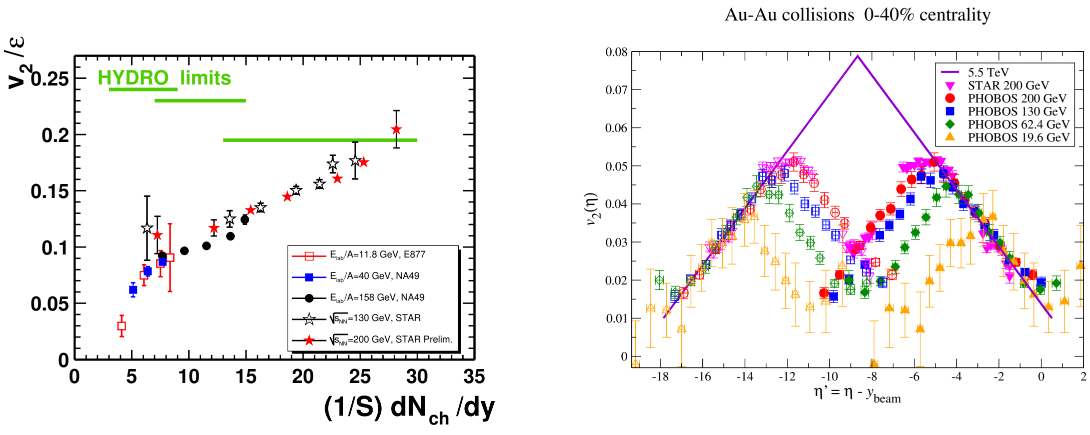

(a) (b)

FIGURE 5. (a) Elliptic flow v_2 normalized to geometrical eccentricity as a function of particle density. (taken from [27]). (b) Elliptic flow v_2 as a function of pseudorapidity, as measured by PHOBOS and reflected about LHC midrapidity (taken from [14]).

The elliptic flow in particular is a powerful probe to investigate the matter produced in relativistic heavy ion collisions at the SPS, RHIC and LHC accelerators. At these energies, the observed elliptic anisotropy is attributed to the presence of a collective motion (flow) of the particles produced in the collision. For non-central collisions, the geometrical anisotropy of the almond-shaped overlap region of the colliding nuclei generates, if enough particle rescatterings occur, a larger pressure gradient in the reaction plane than perpendicular to it [20]. As a consequence, in-plane particles acquire more momentum than out-of-plane particles, leading to a transverse momentum anisotropy that can be observed in the measured particle azimuthal distributions. Since the initial geometrical anisotropy is washed out by the system expansion, the elliptic flow is built in the first stages of the fireball evolution and therefore it brings information on the degree of thermalization, on the time needed to reach the equilibrium and on the shear viscosity of the system created in the nuclear collision [21, 22, 23, 24].

Hydrodynamics assuming ideal (i.e. zero viscosity) fluid and equation of state (EOS) with a first order phase transition is able to explain the measured elliptic flow for central Au-Au collisions at RHIC, as well as its p_T and mass dependence at low p_T [25]. This result is one of the main pieces of evidence for the claim of perfect fluid behaviour of the QGP produced at RHIC. Furthermore, the observed scaling of v_2 with the number of constituent quarks at intermediate p_T [8] supports the presence of a deconfined phase in the early stages of the system evolution.

However, also hints for incomplete thermalization are to be considered [22]. In particular, the measured v_2 normalized to the initial eccentricity (see fig. 5-a) increases with increasing dN/dy in the whole SPS and RHIC energy range, without any hint for a saturation that would indicate the reaching of the hydrodynamic limit (i.e. the v_2/ε value of ideal fluid dynamics). The pseudorapidity dependence of v_2 also supports the out-of-equilibrium hypothesis: the observed extended longitudinal scaling (see fig. 5-b) is naturally accounted for in a scenario with $v_2(\mathrm{y}) \propto \mathrm{d}N/\mathrm{d}y$. The extrapolation of the trends observed in fig. 5 to Pb-Pb mid-central collisions at the LHC gives $v_2(\eta = 0) \approx 0.075$, in contrast with ideal hydrodynamics prediction: $v_2(\eta = 0) \approx 0.06$. The first 20,000 Pb–Pb events at the LHC should allow to clarify the picture.

This possibly incomplete thermalization may be due either to non-zero viscosity in the QGP phase (early viscosity) or to dissipative effects in the hadronic re-scattering stages (late viscosity). Different approaches are being pursued to address the issue of QGP viscosity, for example: eccentricity scaling of v_2 with phenomenological modeling of incomplete thermalization [26], hybrid approach using ideal hydrodynamics to describe the early stages combined with hadronic cascade with dissipative effects in the late stages [23], numerical solution of viscous relativistic hydrodynamic equations [24]. A critical dependence on the initial conditions (either Glauber or Color Glass Condensate, CGC) for the hydrodynamical evolution is found in all these approaches. In particular, for CGC initial conditions (which give significantly larger geometrical eccentricities), the v_2 values measured RHIC seem to favor a scenario with non-zero viscosity in the early partonic phase. The present understanding of the subject allows to claim that the QGP created in central Au–Au collisions at $\sqrt{s}$= 200 GeV behaves as a liquid with exceptionally low viscosity, even if the uncertainty on the initial conditions prevents from making strong quantitative conclusions on its viscosity and its degree of equilibration.

REFERENCES

1. B. B. Back et al. (PHOBOS coll.), Nucl. Phys. A757 (2005) 28.
2. M.C. Abreu et al. (NA50 coll.), Phys. Lett. B 530 (2002), 43.
3. Bialas, Bleszynski and Czyz, Nucl. Phys. B 111 (1976), 461.
4. N. Armesto et al., Phys. Rev. Lett. 94 (2005) 022002.
5. D. Kharzeev, E. Levin and M. Nardi, Nucl Phys A747 (2005) 609.
6. K. Eskola et al., Phys. Rev. C72 (2005) 044904.
7. B. B. Back et al (PHOBOS coll.), nucl-ex/0509034.
8. J. Adams et al. (STAR coll.), Nucl. Phys. A757 (2005) 102.
9. N: Armesto et al., J. Phys. G: Nucl. Part. Phys 35 (2008) 054001.
10. J.D. Bjorken, Phys. Rev. D 27 (1983), 140.
11. I. G. Bearden et al. (BRAHMS coll.), Phys. Rev. Lett. 94 (2005), 162301.
12. K. Adkox et al. (PHENIX coll.), Nucl. Phys. A757 (2005) 184.
13. J. Benecke et al., Phys. Rev. 188 (1969) 2159.
14. N. Borghini and U. A. Wiedemann, J. Phys. G: Nucl. Part. Phys 35 (2008) 023001.
15. M. Basile et al., Phys. Lett. B95 (1980) 311.
16. B. B. Back et al nucl-ex/0301017 v1
17. A. Andronic et al., Nucl. Phys. A772 (2006) 167.
18. F. Becattini and U. Heinz, Z. Phys. C76 (1997) 269.
19. R. Hagedorn, Suppl. Nuovo Cimento 3 (1965) 147.
20. J. Y. Ollitrault, Nucl. Phys. A638 (1998) 195.
21. U. Heinz, J. Phys. G31 (2005) S717.
22. R. S. Bhalerao, J. P. Blaizot, N. Borghini and J. Y. Ollitrault, Phys. Lett. B627 (2005) 49.
23. T. Hirano, U. W. Heinz, D. Kharzeev, R. Lacey and Y. Nara, Phys. Lett. B636 (2006) 299.
24. M. Luzum, P. Romatschke, Phys. Rev. C78 (2008) 034915.
25. U. Heinz and P. F. Kolb, Nucl. Phys. A702 (2002), 269c.
26. H. J. Drescher et al., Phys. Rev. C76 (2007) 024905.
27. C. Alt et al., NA49 coll., Phys. Rev. C68 (2003) 034903.